ReadMe
HVAB Thermography Data

Avraham S. Gileadi
NASA Ames Research Center
September 2023

The following text is largely extracted from Norman et al., "Fundamental Test of a Hovering Rotor: Comprehensive Measurements for CFD Validation," Vertical Flight Society's 79th Annual Forum & Technology Display, West Palm Beach, FL, USA, May 16-18, 2023.

This document outlines the conditions under which the thermography data was collected, along with the methods used to process the images into a final, usable form. Additionally, it provides a description of the naming convention and content for all outputs.

Thermography Test Description

The test was conducted in the NFAC 80- by 120-Foot Wind Tunnel test section using an 11.08-ft diameter rotor system mounted on the Army Rotor Test Stand (ARTS). The rotor plane was located 6.4 in above the tunnel centerline (480.4 in above the acoustically treated floor) and centered between the two tunnel sidewalls.

Table 1. HVAB Rotor Parameters

Parameter	Value
Number of blades	4
Radius, in	66.50
Blade chord, in	5.45
Rotor Geometric Solidity	0.1033
Rotor Airfoil	RC series
Blade Twist	Linear, -14 deg

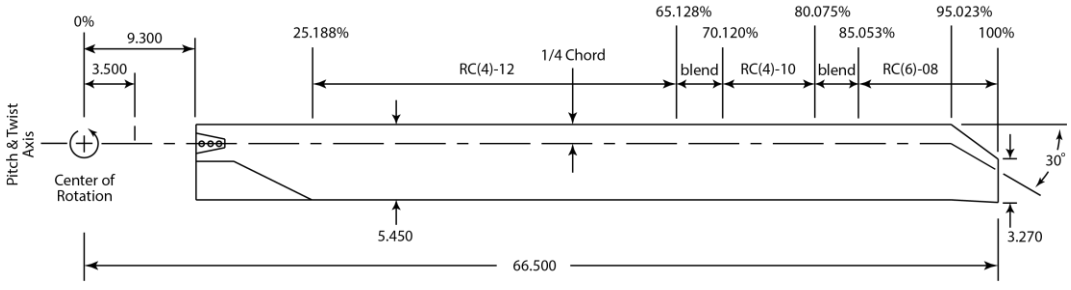

Figure 1. HVAB blade planform.

A radially aligned rotating mirror, with its spin axis closely aligned to the rotor spin axis and rotating at half the speed of the rotor, allows the virtual image of a blade to remain fixed on the camera sensor. This "freezing" of the image of the passing blade permits longer exposure times without incurring motion blur. A FLIR X8501sc camera with a 1280 X 1024 Strained Layer Superlattice (SLS) sensor and fitted with a 100mm f2.3 lens was used in conjunction with each rotating mirror system. This camera is sensitive from 7.5 to 11 microns, which is near the peak of the Planck curve at room temperature. One mirror/camera assembly was installed in the attic of the wind tunnel to visualize the blade upper surface. The camera for this system peered through an anti-reflection coated Germanium window to prevent debris from falling into the rotor disk. The second assembly was mounted on the test section floor to visualize the lower blade surface. Figure 2 shows the installation of both systems (note the triangular shaped Germanium window in the attic-mounted assembly). The cameras captured images when the blades were aligned with the tunnel centerline at the nominal 0° rotor azimuth position.

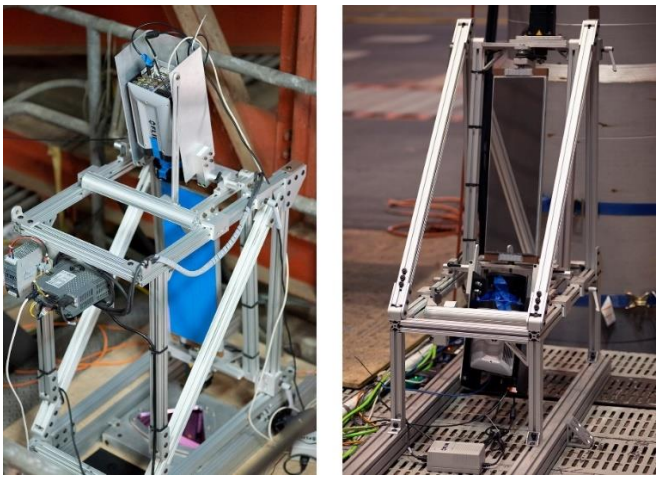

a) b)

Figure 2. Thermography system showing a) upper surface camera in the attic, b) lower surface camera on the test section floor.

The blades were coated with high-emissivity black polyurethane paint to improve thermal image quality, and then buffed to a surface roughness of less than 10 microinches (rms). Fiducial targets of gold ink (0.5 in diameter) were applied to all blade surfaces, spaced two inches apart and inset one inch from the leading and trailing edges. These low emissivity targets were added to allow for blade image alignment and averaging during post-processing. Fifty images of each blade were acquired at each test condition during operations to allow for this averaging.

Image Processing

Each set of 50 images was stored as a FLIR-proprietary *.ats file, which concatenates each raw image and stores their thermal and grayscale data. Each image must be exported to a .tif file after rendering the 16-bit image data as a suitable 8- bit display. The images were rendered with as much pertinent grayscale data as practical. Further image processing was done to enhance the sharpness and contrast.

The averaging process required that the fiducial targets in each image be located to subpixel accuracy. This was accomplished using the same target-finding and correction utility as was used for photogrammetry.

Additionally, a method for enhancing the contrast of the entire blade was developed. The images exhibited a large root-to-tip increase in brightness because of the increasing local Mach number and recovery temperature. In contrast, differences due to laminar and turbulent boundary layers were very small and were especially difficult to see inboard where the images were very dim. The contrast between laminar and turbulent regions was enhanced by first scaling the images radially to minimize the large root-to-tip brightness gradient. Then the image brightness levels were scaled between the relatively small difference in brightness between darker laminar and brighter turbulent regions. After this adjustment, contrast between laminar and turbulent regions was much greater and was approximately uniform from root to tip. Figure 3 shows a sample blade image through this workflow.

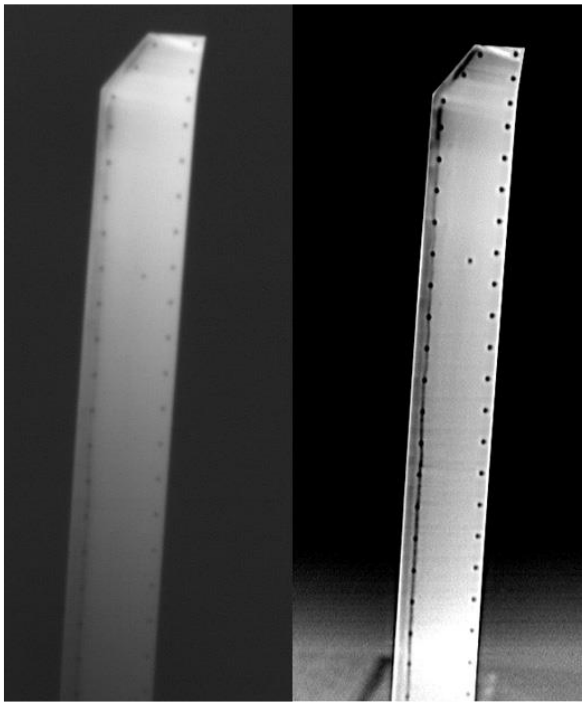

a) b)

Figure 3. Example of the effect of image processing steps for a single blade image. a) Sample of an image exported from the *.ats raw file and b) final image after sharpening, averaging, and applying the dual-slope contrast enhancement.

Transition of the boundary layer from laminar to turbulent was assumed to occur at the interface between dark laminar and brighter turbulent regions. The chordwise position of this interface at each radial station was assumed to occur where the gradient of image brightness was greatest. An automatic algorithm was developed to locate this position at all radial stations, resulting in a line of transition from root to tip. The algorithm also found the leading and trailing edges of the blade at each station to compute the normalized position of transition from the leading edge (x/c). The normalized radial position (r/R) of each chordwise row was scaled from the known image and space coordinates of the tip

and targets along the leading edge. The normalization assumes the blade is essentially 2D and does not attempt to account for leading edge geometry. By using the leading and trailing edges in each image, the normalization algorithm accounts for the blade angle in its calculation.

Figure 4 shows how the transition line was determined from the chordwise grayscale intensity, its derivative showing the peak of the gradient, and the line of chordwise peaks of this gradient superimposed on an image. These traces are smoothed using a cubic spline with a smoothing factor – the random noise of the image data made for a non-physical, jagged appearance of the transition lines.

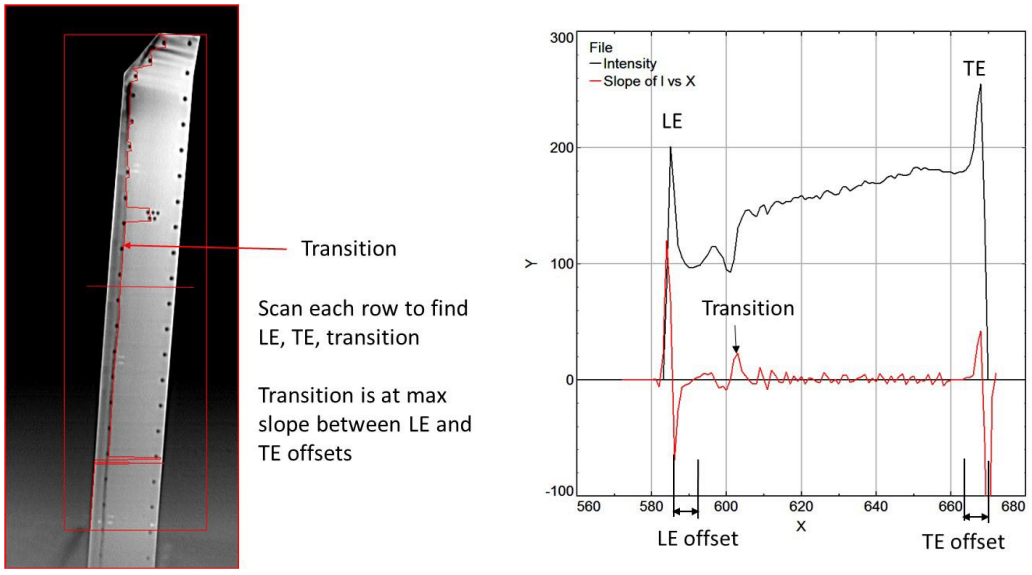

a) b)

Figure 4. Plots showing the derivation of the chordwise location of the transition. a) Trace of the transition line on the blade. b) Intensity vs. Chord and Derivative of Intensity vs. Chord.

When processing the data across multiple tip Mach numbers and collectives, the performance of the tracing algorithm was frequently degraded by the presence of the fiducial targets. To address this issue, an OpenCV inpainting algorithm was implemented to remove the targets from the images. Inpainting was initially developed to remove scratches and other artifacts in images and works by replacing masked areas with pixels created from its neighbors. In the thermography datasets, the targets were first located using the same software used for photogrammetry. Then a program was developed that masked out each of the targets, replacing them with a weighted sum of all known pixels in the neighborhood. Results are shown in Figure 5. While the method did not remove all evidence of the targets, it allowed the transition tracing algorithm to operate more effectively and increased the quantity of useable data.

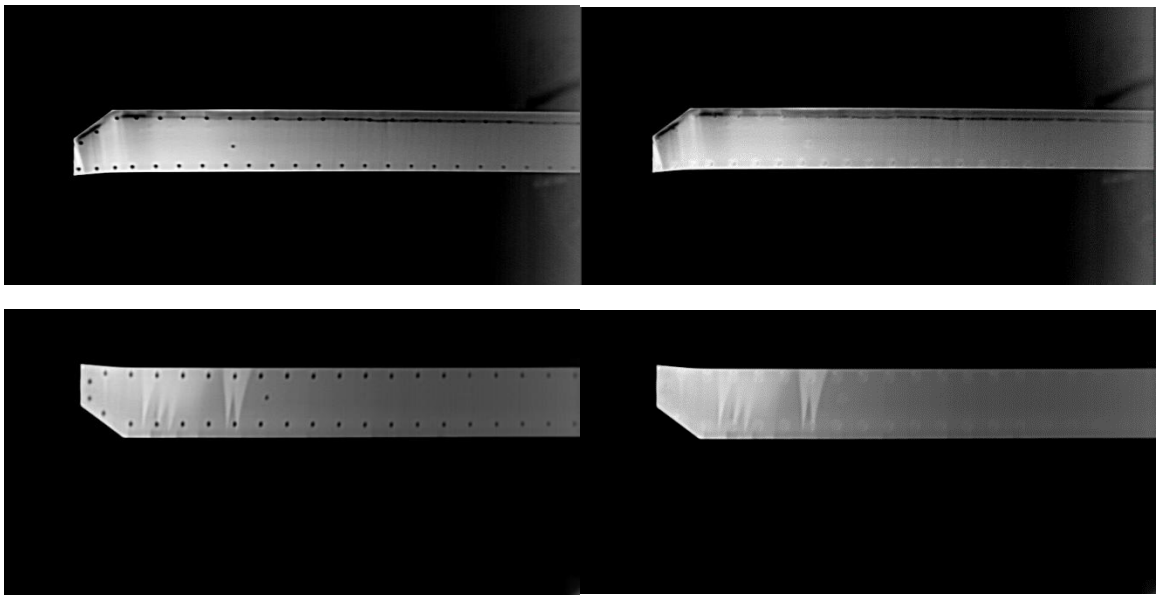

a) b)

Figure 5. Examples of images with the targets removed using inpainting. a) Original enhanced images. b) Same images with inpainted targets.

Despite removal of the targets, the tracing algorithm would sometimes locate the transition on the artificial intensity gradients present because of the inpainting. By inspection, the data was deleted in areas where the tracing algorithm incorrectly identified inpainted targets as the location of transition. The deleted data was "filled-in" using interpolation fit to a cubic spline. The image in Figure 6 shows the results of the editing process for a representative upper blade. The blue line is the original trace, and the red line is the edited result. It was observed that the quality of the transition data degraded as the images approached the root of the blade. As a result, the images and datasets needed to be cropped/truncated.

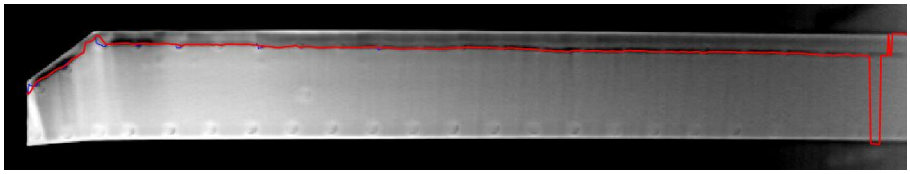

Figure 6. Example of upper blade with original (blue) and edited (red) traces plotted.

Observations on the Results

The upper surface images are consistent with one another. The lower surface images show mostly laminar flow except for wedge shaped regions, possibly caused by surface contamination. The locations of the wedges are different for each blade and often change location between runs (the blades were cleaned before every run). The shape of these wedges is interesting in that the wedge angle begins very narrow in the laminar region. As the boundary layer approaches the trailing edge and the region of adverse pressure gradient measured in the pressure distributions, the wedge angle grows wider

indicating the transition process is already occurring before the trailing edge. It becomes difficult to visualize transition in this region owing to the low values of skin friction and the likely more gradual amplification of the Tollmien-Schlichting waves.

Additional challenges were encountered when processing a wider range of data. There are processing artifacts within the images not tied to physical phenomena. Sharpening an image is known to create artificial effects near edges. Sharpening the blade images results in an artificial dark band just inside the leading and trailing edges. In cases where a strong transition line was not present (such as found on the lower blades), the tracing algorithm would incorrectly locate the transition on the dark bands or on the infilled targets.

On the lower blades, the relatively strong intensity gradients from the wedge-shaped transitions and processing artifacts rendered the tracing algorithm largely ineffective. Accounting for these challenges algorithmically will require more advanced tools and further development. As a result, no transition data is provided for the lower surface, only the clean un-traced images are provided.

Description of Data

The data is named using the following convention: R##MXXXTHYYZ where ## is replaced with the run number, XXX the tip Mach number, YY with the collective angle, and Z with U or L for the upper or lower blade surface respectively.

The following data is delivered for each run. It is assumed that each of the items below is preceded with the data name.

- .txt – contains the normalized data for each blade. First column is r/R, second column is x/c, and the third column is the blade serial identifier (i.e. b1 for blade 1).
- _averaged.txt – this file is the average of each of the four blades. First column is r/R, second is x/c.
- _clean.bmp – The four concatenated blade images with blade 1 on the top and blade 5 on the bottom.
- _data.bmp – the same images as _clean.bmp but with the edited traces overlayed on top.
- _traces.png – a plot of the normalized and averaged data from four blades from the .dat files.
- _traces_ave3std.png – a plot of the averaged normalized data on top of the standard deviation for the data. The red lines extend 3 standard deviations above and below the average. While the reliability and confidence is low for a four datapoint data set (on the order of 70% confidence with 75% reliability), the charts provide an easy to follow visual of the deviation present within the datasets.